AIP Advances

Construction of a magnetic bottle spectrometer and its application to pulse duration measurement of X-ray laser using a pump-probe method

Cite as: AIP Advances **5**, 117101 (2015); https://doi.org/10.1063/1.4935260
Submitted: 09 June 2015 . Accepted: 22 October 2015 . Published Online: 02 November 2015

S. Namba, N. Hasegawa, M. Kishimoto, M. Nishikino, M. Ishino, and T. Kawachi

ARTICLES YOU MAY BE INTERESTED IN

AIP Advances **5**, 117101 (2015); https://doi.org/10.1063/1.4935260 **5**, 117101

AIP ADVANCES **5**, 117101 (2015)

Construction of a magnetic bottle spectrometer and its application to pulse duration measurement of X-ray laser using a pump-probe method

S. Namba,[1,a] N. Hasegawa,[2] M. Kishimoto,[2] M. Nishikino,[2] M. Ishino,[2] and T. Kawachi[2]
[1]*Graduate School of Engineering, Hiroshima University, 1-4-1 Kagamiyama, Higashi-hiroshima, Hiroshima 739-8527, Japan*
[2]*Quantum Beam Science Directorate, Japan Atomic Energy Agency, 8-1 Umemidai, Kizugawa, Kyoto 619-0215, Japan*

(Received 9 June 2015; accepted 22 October 2015; published online 2 November 2015)

To characterize the temporal evolution of ultrashort X-ray pulses emitted by laser plasmas using a pump-probe method, a magnetic bottle time-of-flight electron spectrometer is constructed. The design is determined by numerical calculations of a mirror magnetic field and of the electron trajectory in a flight tube. The performance of the spectrometer is characterized by measuring the electron spectra of xenon atoms irradiated with a laser-driven plasma X-ray pulse. In addition, two-color above-threshold ionization (ATI) experiment is conducted for measurement of the X-ray laser pulse duration, in which xenon atoms are simultaneously irradiated with an X-ray laser pump and an IR laser probe. The correlation in the intensity of the sideband spectra of the 4*d* inner-shell photoelectrons and in the time delay of the two laser pulses yields an X-ray pulse width of 5.7 ps, in good agreement with the value obtained using an X-ray streak camera. [http://dx.doi.org/10.1063/1.4935260]

I. INTRODUCTION

Laser-produced plasmas (LPPs) are expected to be a compact and bright light source in the vacuum ultraviolet (VUV) and soft X-ray regime.[1,2] Even hard X-rays up to 20 keV (gold Kα) caused by energetic electrons in an LPP can be obtained by irradiating a bulk target with intense laser pulses.[3] Research in physics,[4,5] chemistry,[6] and biomedical science[7,8] using alternative X-ray sources has been carried out. As an application of LPP X-rays to radiation biology, short-pulse copper (Cu) Kα X-ray pulses (of width 1 ps with $h\nu = 8$ keV) have been used to irradiate a biological cell. Such X-rays can exert an influence on cell nuclei that is similar to those obtained using conventional X-ray tubes and linear accelerators.[9,10] However, shorter pulse X-rays are required to investigate ultrafast chemical reactions within a cell, typically in the femtosecond time domain.

On the other hand, by irradiating xenon (Xe) atoms with intense short-pulse X-rays, an extremely excited state having multiple vacancies in the inner shell can be populated. The energy threshold for photoionization of Xe 4*d* inner electrons is about 70 eV. The inner hole immediately decays into stable states on the femtosecond time scale by an Auger process.[11] Thus, an intense X-ray pulse with a photon energy sufficient to ionize the inner-shell electron and with a short pulse duration is needed to create multiple inner-ionized atoms. Although the temporal behavior of the X-rays has to be accurately determined, a conventional streak camera is not applicable to femtosecond X-ray pulses, because its time resolution is limited to ~1 ps.

In order to evaluate the temporal characteristics of the X-rays in the subpicosecond domain, Woerkom *et al.*[12] and Schins *et al.*[13] adopted a cross-correlation technique as pump-probe spectroscopy.

---

[a] Corresponding author: Shinichi Namba (namba@hiroshima-u.ac.jp)

In this method, first, an X-ray *pump* pulse ionizes the inner- and outer-shell electrons. When an optical *probe* pulse is irradiated in the interaction region, the electrons absorb or emit the photons, resulting in sideband spectra at frequency shifts $\pm h\nu_{\text{probe}}$ relative to the main peak (two-color above-threshold ionization (ATI)[14]). By analyzing the correlation amplitudes of the sideband spectra and the time delay between the ionizing pump and the dressing probe pulses in the perturbative regime, the pulse shape of the pump X-ray beam can be determined. In principle, the time resolution is limited by the electron transit time through the interaction region of both lasers and of the gas target.

Using a similar technique, attosecond XUV pulses can also be characterized. Itatani *et al.* proposed a novel method to determine the pulse duration in the attosecond time domain, in which the energy and angular distribution of photoelectrons in the presence of a strong infrared (IR) femtosecond laser field are measured.[15] The key to the method is the phase between the XUV ionizing pump pulse and the carrier wave (*not* the envelope) of the IR laser pulse for dressing the electron. The method has been demonstrated for a single attosecond laser pulse by Hentschel *et al.*.[16] In that study, the cross correlation of high-order harmonics in the XUV regime with a few-cycle probe pulse was measured to evaluate the temporal characteristics of an XUV pulse.

To measure the cross correlation associated with the pump-probe method, a spectrometer capable of measuring an electron spectrum in a single shot with high energy resolution is essential. In the present study, therefore, a magnetic bottle time-of-flight (TOF) electron spectrometer is constructed.[17–19] The advantages of the spectrometer are: (1) single-shot measurements, (ii) simple structure compared with a concentric hemispherical analyzer (CHA) and cylindrical mirror analyzer (CMA), (iii) large collection angle (almost 4π), and (iv) high energy resolution. In order to investigate electron trajectories in the field formed by a permanent magnet and a solenoid coil, and to determine the detection efficiency, a numerical calculation using a finite-element method is performed. Experimentally, the energy resolution of the spectrometer is determined by measuring the electrons emitted by Xe atoms irradiated with a laser-driven plasma X-ray pulse. As the pump-probe experiment, the pulse width of the plasma X-ray laser is measured. The full width at half maximum (FWHM) of the laser pulse is found to be 5.7 ps, in agreement with the temporal profile measured by an X-ray streak camera.

II. DESIGN AND CONSTRUCTION OF THE MAGNETIC BOTTLE SPECTROMETER

Figure 1(a) presents a schematic of the magnetic bottle TOF electron spectrometer. The magnetic mirror field is generated by a tapered permanent magnet and a solenoid. The strength of the permanent magnet (made of neodymium with a diameter of 20 mm, a length of 30 mm, and a taper angle of

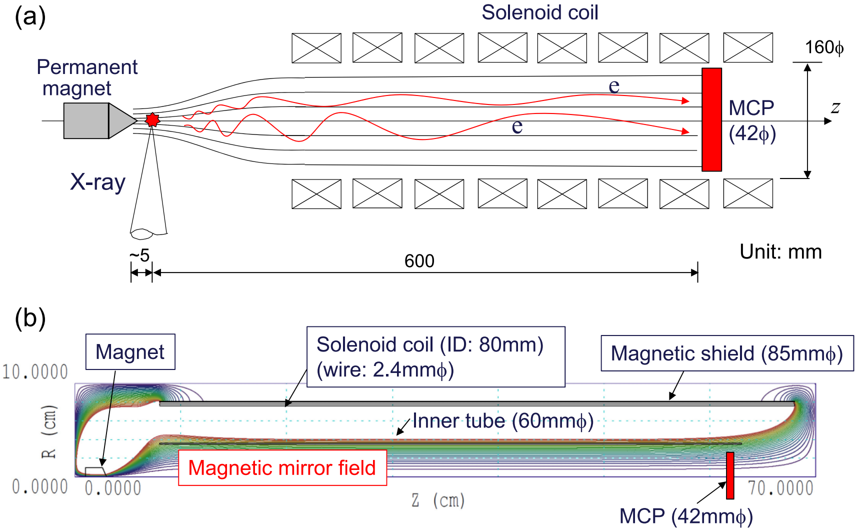

FIG. 1. (a) Schematic of the magnetic bottle TOF electron spectrometer. (b) Contour plot of the stream function rA_θ of the magnetic field calculated using a finite-element method.

110°) is 0.25 T at the taper tip (z = 30 mm). A weak uniform field of 10 mT is applied by the coil that is wound on an 80-mm diameter stainless steel tube. The wire diameter is 2.4 mm (made of 2.0-mm copper with an outer insulator that is 0.4 mm thick) and the coil length is 600 mm (with 250 turns). The current in the coil is 2 A. The magnetic field outside the vacuum tube is shielded by nanocrystalline soft magnetic material sheets (FINEMET® from Hitachi Metal). A microchannel plate (MCP, Hamamatsu Photonics, F9892-11), having an effective diameter of 42 mm, is located 600 mm away from the laser focal point. The MCP rise time is 1.2 ns (FWHM). The relative positions of the magnet, focal point, and introduced gas nozzle are optimized by using a customized MCP having a phosphor plate (Hamamatsu Photonics, F2225-21P447).

The electrons are generated a few millimeters downstream from the permanent magnet (at z = 35 mm), where the Xe atoms are irradiated with a soft X-ray laser pulse. Almost all the electrons can reach the detector due to the guidance along the mirror magnetic field. To calculate the magnetic field in the TOF tube, a numerical calculation is performed using a finite-element method. Figure 1(b) is a contour plot of the field strength rA_θ (i.e., the stream function) generated by the magnet and the solenoid, where r is the radius and A_θ is the vector potential. A smooth magnetic mirror field is formed in the flight tube.

The trajectory of electrons in the field is calculated by solving the equations of motion. Figure 2 plots the electron positions at the MCP detector (in an xy projection), when 2500 electrons with a kinetic energy of E = 20 eV are isotropically emitted from the 500-μm spherical spot at the focal position of z = 35 mm indicated by the black circle. The influence of the space charge on the electron energy is not taken into account. The electrons are guided into the effective area of the detector, although they spatially spread out to a diameter of 15 mm, depending on their initial emission angle and position.

Figure 3(a) shows the electron TOF spectra calculated for various kinetic energies. The emission conditions are the same as those in Fig. 2. The initial energy spread is assumed to have a Gaussian profile with a FWHM of ΔE = 0.5 eV. Even at 80 eV, the electrons are efficiently collected by the detector. No significant spectral distortion is observed for low-energy electrons, while at high energies the distribution splits and becomes asymmetric. The TOF spectrum depends on various parameters such as the kinetic energy, the length of the drift region, the angular distribution, the pulse duration of the incident laser, the laser spot size, and the magnetic field. In particular, the nonuniform magnetic

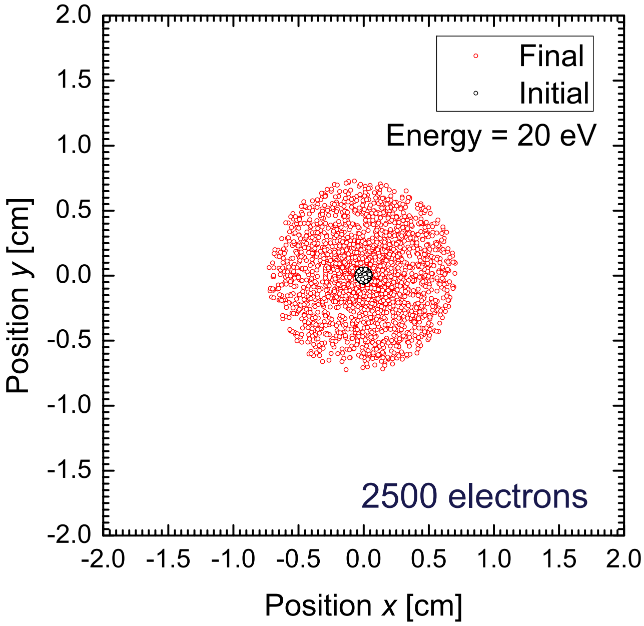

FIG. 2. Spatial distribution of electrons at the MCP detector. The electrons have a kinetic energy of E = 20 eV; 2500 particles are isotropically emitted at z = 35 mm from a 500-µm sphere. The energy distribution is Gaussian with a FWHM of 0.5 eV.

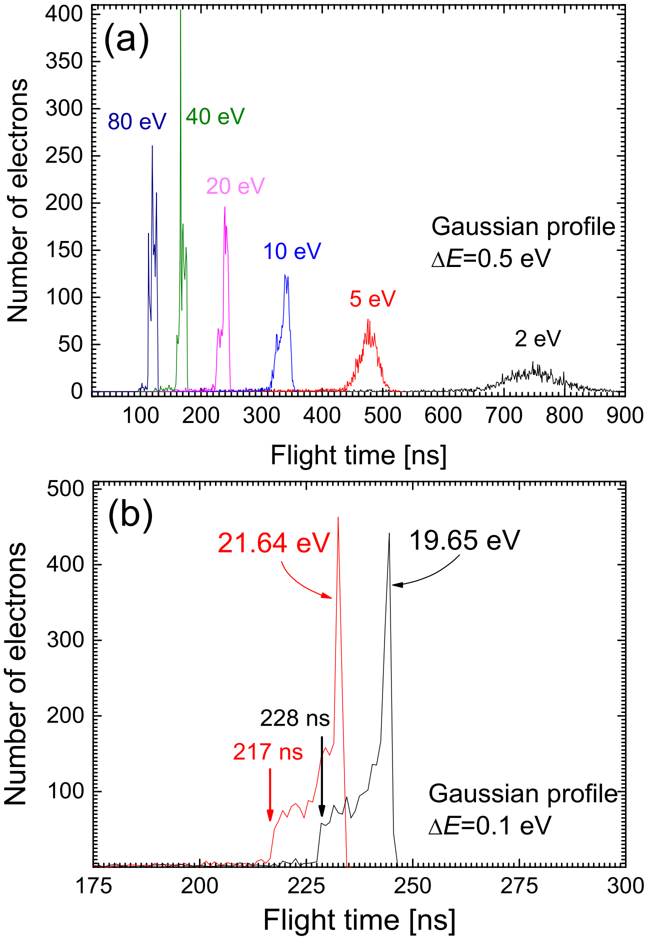

FIG. 3. (a) Electron TOF spectra for various kinetic energies. (b) Photo-electron spectra associated with Xe 4*d* inner-shell ionization by 89.2-eV X-ray irradiation. The number of electrons emitted by the 500-µm sphere is 2500.

field alters the Larmor radius of the drifting electrons, resulting in the complicated TOF spectrum. This effect is more pronounced for higher energy electrons due to their larger orbits.

Figure 3(b) plots the TOF spectra calculated for 21.64- and 19.65-eV electrons. Those respective energies correspond to transitions for $4d\ j = 5/2$ and 3/2 photoelectrons generated by 89.2-eV X-ray irradiation of Xe atoms, as will be described later. It is assumed that the electron energy distribution has a Gaussian profile with a FWHM of 0.1 eV, which describes the lifetime of a 4*d* inner vacancy.[11] The arrows at 217 and 228 ns are the flight times evaluated from the path excluding the Lamor motion and the kinetic energies for 21.64 and 19.65-eV electrons, respectively.

III. PERFORMANCE OF THE SPECTROMETER

A. Generation of electrons by a bright X-ray source

In order to characterize the magnetic bottle spectrometer, we measure the electron energy spectra of Xe atoms subjected to the laser-driven plasma soft X-ray laser at the Japan Atomic Energy Agency (JAEA).[20] The laser wavelength and photon energy are 13.9 nm (bandwidth $\Delta\lambda/\lambda \leq 10^{-4}$) and 89.19 eV, respectively, corresponding to the 4*d*–4*p* transition of nickel-like silver ions. The pulse width is measured to be 8 ps using an X-ray streak camera.[21,22] The repetition rate of the laser is 0.1 Hz.[23] Broadband radiation emitted by the laser plasma is filtered by a 200-nm-thick zirconium filter so that monochromatic laser light is obtained. The laser spot diameter and the highest intensity

TABLE I. Representative electron energies associated with $5p$ outer- and $4d$ inner-shell ionizations and subsequent Auger decay processes. The cross section for photo-ionization and the relative intensity of the Auger lines are also listed.

	energy [eV]	flight time	cross section [Mb] [25,27]	relative intensity[26]
Auger electrons	8.26	352.29		224
	10.25	316.25		136
	12.72	283.89		36
	14.69	264.17		36
	16.12	252.18		120
	17.23	243.92		49
	21.65	217.60		65
	31.95	179.13		141
	32.33	178.07		150
	33.23	175.64		44
	34.45	172.50		119
	35.21	170.63		50
photo-electron $4d$ $j = 3/2$	19.65	228.41	9.57	—
$4d$ $j = 5/2$	21.64	217.65	12.43	—
$5p$ (outer shell)	77.05	115.35	1.50	—

focused by a concave Mo/Si multilayer mirror (having a radius R = 1000 mm) are about 40 µm and $\leq 5\times10^8$ W/cm^2, respectively.

As targets, two Xe gas feeding systems are used: (1) a variable leak valve to fill the atoms in the interaction region through a 0.14-mm-diameter needle, and (2) an effusive pulsed atomic beam created by expanding low-pressure gas through an electromagnetic valve. In the former case, the needle is installed just below the focal point, whereas in the latter the distance between the laser focal point and the valve is 150 mm and a 0.5-mm-diameter skimmer is used to collimate the atomic beam and improve the energy resolution.

The laser photon energy is high enough to photoionize Xe $4d$ core electrons (thresholds: 69.54 and 67.55 eV for spin-orbit states j =3/2 and 5/2, respectively[24]). The cross section at 90 eV is as large as 22 Mb due to a giant resonance, while for outer shell it is only 1.5 Mb.[25] Table I lists representative electron energies associated with the outer- and inner-shell ionizations and subsequent Auger decay processes.[26] The cross section for j = 3/2 and 5/2 are evaluated by taking the branching ratio into account.[27] The relative intensities for the Auger transitions are also tabulated.[26]

B. Alignment of the spectrometer and photo-ionization area

To optimize the energy resolution and collection efficiency, the permanent magnet and focal point of the laser need to be positioned appropriately. For this purpose, the MCP assembly with a phosphor is used, which permits simultaneous observation of the electron positions on the screen and the TOF signal. Figure 4 illustrates various time-integrated images on the screen obtained by using the needle gas feeder for different positions of the permanent magnet. The atoms on the laser axis are ionized throughout the Rayleigh length of ~50 mm, resulting in longer images along the x axis than along the y axis. By adjusting the position of the magnet, focusing mirror, and gas needle, the optimal condition in panel (c) is obtained, so that the electron energy spectrum can be measured with high temporal resolution.

C. Electron TOF spectra and kinetic energy distribution

The TOF signal for Xe $4d$ spin-orbit states, Auger transitions and $5p$ outer-shell states is plotted in Fig. 5(a). The MCP detector without a phosphor screen and the pulsed Xe atomic beam are used, to ensure a faster time response and a higher energy resolution. This TOF spectrum is different from the calculated curve in Fig. 3(b). The time width for $4d_{3/2}$ photoelectrons is measured to be 6.5 ns,

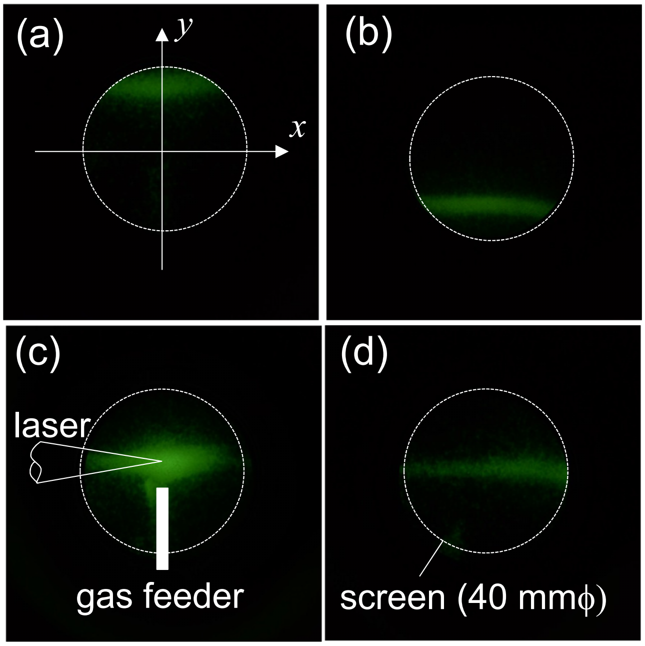

FIG. 4. Electron images on the phosphor screen for a permanent magnet position of (a) $x = 0.0$ mm, $y = 1.0$ mm, (b) $x = 0.0$ mm, $y = -1.0$ mm, (c) $x = 0.0$ mm, $y = 0.0$ mm, and (d) $x = 1.0$ mm, $y = 0.0$ mm.

which is much longer than the calculated value of 2.3 ns for the 245-ns main peak. The temporal resolution expected from the 0.5-mm spatial extent of the gas target is negligibly small: about 200 ps for 20-eV electrons. The result indicates that space charge broadens the electron spectra.[28,29] For example, assuming that the laser intensity is 5×10^8 W/cm^2 and the atomic density is 10^{12} cm^{-3}, 10^{10} electrons can be generated within a 40-μm-diameter spot during the laser pulse. Therefore, with decreasing the laser intensity and gas density, the time width (energy resolution) becomes narrower. In fact, the time width is as narrow as 3 ns for 245-ns peak under a laser intensity of $\sim5\times10^7$ W/cm^2 and Xe density of $\sim10^{10}$ cm^{-3}, as shown in the inset of FIG. 5(a).

Figure 5(b) graphs the electron energy distribution function $f(E)/E^{3/2}$. The sensitivity of the spectrometer is not calibrated and thus low-energy electrons being less sensitive. The photoelectron peaks attributed to $4d^{-1}$ and $5p^{-1}$ states, and the Auger lines associated with the inner vacancy can be readily assigned. The spectral width of the $4d$ $j = 3/2$ line (at E = 19.65 eV) is about 1.0 eV, whereas for the 8.26-eV Auger peak it is significantly improved to ΔE = 0.45 eV due to the longer flight time for slower electrons. For the condition of laser intensity of $\sim5\times10^7$ W/cm^2 and Xe density of $\sim10^{10}$ cm^{-3}, the width of 19.65-eV peak is 0.66 eV due to suppression of the space charge effect, as shown in the inset of FIG. 5(b).

IV. APPLICATION TO X-RAY PULSE WIDTH MEASUREMENT BY PUMP-PROBE SPECTROSCOPY

By analyzing the electron energy spectra in the pump-probe experiment, the pulse width of the laser-driven X-ray laser is characterized. Two Nd:glass laser systems having a common oscillator and regenerative amplifier are used for this purpose.[23] One generates the X-ray laser beam, while the other synchronizes with the X-ray laser beam and is used as the IR probe beam. The probe pulse has a wavelength of 1053 nm (corresponding to $h\nu$ = 1.18 eV) and a pulse width of ~2 ps. It is focused onto the photo-ionization area using a 1000-mm focal-length lens (intensity: 10^{12} W/cm^2). The pump X-ray laser and the IR probe pulse intersect at a certain time delay, when the Xe atom is photo-ionized by the X-rays, and the photo- and Auger electrons are dressed by the probe light. Consequently, the electrons emit or absorb the infrared photons, so that sidebands with a separation of 1.18 eV appear on both sides of the main peak.

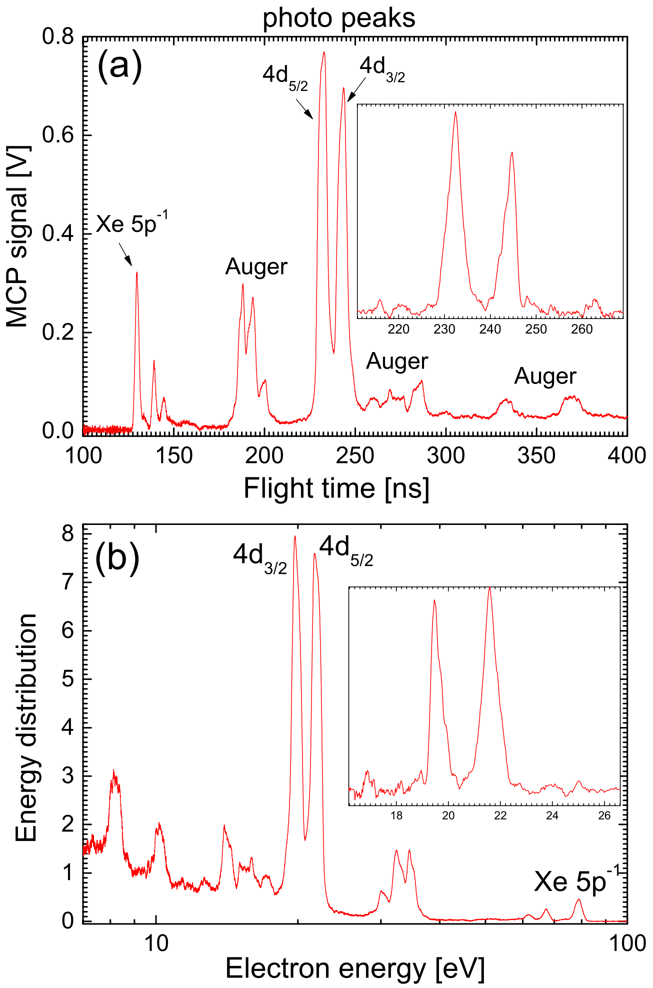

FIG. 5. (a) Electron TOF spectrum of Xe atoms irradiated with an 89.2-eV X-ray laser pulse. (b) Energy distribution function. Photo-electron and Auger peaks following 4*d* photo-ionization are observed. The insets represent the data obtained for laser intensity of ~5×10^{7} W/cm^{2} and Xe density of ~10^{10} cm^{-3}.

The sidebands corresponding to the Auger spectrum provide favorable conditions for evaluating the cross correlation. In particular, the Auger peak at 8.26 eV and the dressed sideband at 7.08 eV are a promising pair, because the spectrum in the low-energy region has a higher resolution. Moreover, the Auger line can also be used for pulse width measurements of continuum radiation. Note that the line shape of the photoelectron spectrum broadens if monochromatic X-rays are not used, whereas the kinetic energy of the Auger electrons is independent of the photon energies of the pump X-rays. In reality, however, the sideband signal attributed to Auger electrons is small, and thus the TOF spectra have to be accumulated over thousands of laser shots. That kind of accumulation is not practical for the current laser system, because the repetition rate of the X-ray pulse is only 0.1 Hz. In this study, therefore, we focus on the sideband spectra accompanying the 4*d* photoelectrons.

Kroll and Watson have derived the differential cross section for *n* IR photon exchanges with absorption ($n < 0$) or stimulated emission ($n > 0$) in laser-assisted potential scattering process.[30] If the electron energy is significantly higher than that of the probe photon, the soft photon approximation[31] is applicable to calculate the differential cross section for the single X-ray and *n* IR photons absorptions, that is,

$$\frac{d\sigma_n}{d\Omega} = J_n^2(x)\frac{d\sigma_0}{d\Omega}, \qquad (1)$$

where $J_n(x)$ is a Bessel function and the argument is $x = -e\boldsymbol{a}\cdot(\boldsymbol{p}-\boldsymbol{p}_0)/mch\nu_{IR}$ for $\boldsymbol{a}$ vector potential of the IR pulse and $\boldsymbol{p}_0$ and $\boldsymbol{p}$ are the momentums of the initial and final (dressed) electronic states. The differential cross section in the absence of the IR dressing field, $\frac{d\sigma_0}{d\Omega}$ is given by,[32]

$$\frac{d\sigma_0}{d\Omega} = \frac{2^4\alpha(pa_0)^3}{\pi m_e\nu_{IR}}\frac{cos^2\theta}{\left(1+p^2a_0^2\right)^4}, \tag{2}$$

where α is the fine structure constant, a_0 is the Bohr radius and θ is the angle between the polarization direction of the laser beam and the emitted electron. By substituting Eq. (2) to (1) and integrating with respect to the angle θ, the transition probability of two-color ATI process can be calculated. Figure 6(a) plots the spectra of 21.64-eV photoelectron and accompanying sidebands for various probe laser intensities. Above the laser intensity of 10^{11} W/cm^2, the sideband spectra appear at both sides of the main photo peak. In reality, the energy peaks of $4d\ j = 3/2$ (19.65 eV) and 5/2 (21.64 eV) photoelectrons are close together and thus the resultant spectra become complicated, as shown in FIG. 6(b). Moreover, the low-energy resolution of $\Delta E = 0.66$ eV around 20-eV energy makes it difficult to decompose the $n = \pm1$ sidebands from the main peaks. So instead, attention is focused on the n = -2 spectrum for $j = 5/2$ at $E = 24.0$ eV.

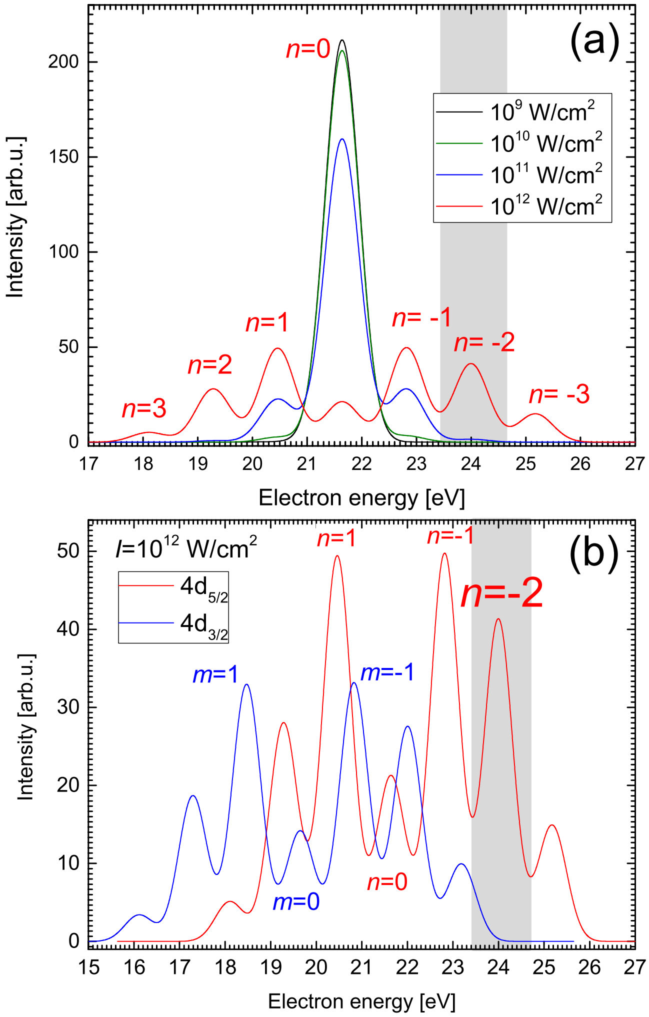

FIG. 6. (a) Calculated two-color ATI transition probability of 21.64-eV photoelectron for various probe intensities. At 1×10^{12} W/cm^2, 3 photon exchange processes ($n = \pm3$) are clearly seen. (b) Complicated spectra are expected around 20 eV at a probe intensity of 1×10^{12} W/cm^2, because the 19.65-eV and 21.64 eV energy peaks are close together.

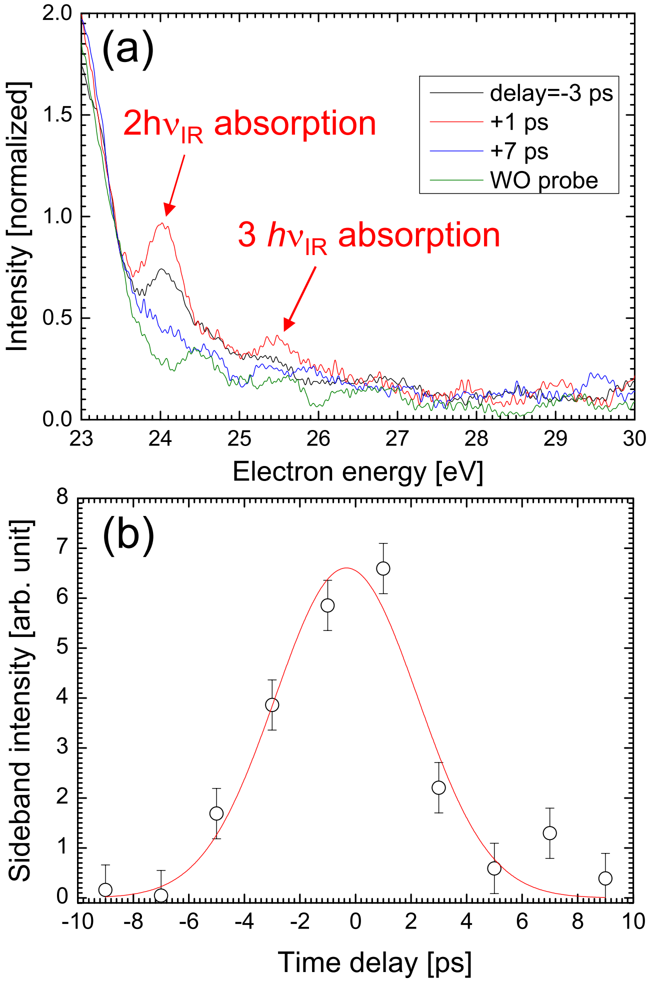

FIG. 7. (a) Electron energy spectra observed for various time delays of the IR probe pulse relative to the X-ray laser pump. Two and three IR photon absorption lines are observable for the temporal overlap between both X-ray and IR pulses. (b) Distribution of the sideband intensity on time delay yields an X-ray pulse duration of 5.7 ps.

Figure 7(a) graphs the energy spectra relevant to this process for various time delays. Around zero time delay, a prominent peak attributed to IR two-photon absorption ($2h\nu_{\mathrm{IR}}$) is observed. The temporal variation of the sideband intensity is plotted in Fig. 7(b). Assuming that the instrumental width is given by the temporal profile of the Gaussian probe pulse, the X-ray pulse width is found to be 5.7 ps FWHM, in good agreement with the value measured using the X-ray streak camera.

V. SUMMARY

A magnetic bottle electron spectrometer has been developed for pump-probe experiments, providing the means to measure the temporal behavior of an ultrashort X-ray pulse. The performance of the spectrometer has been characterized by irradiating Xe atoms with a plasma X-ray laser pulse. The energy resolution for 8.26-eV Auger electrons, following photo-ionization of $4d$ electrons, was determined to be 0.45 eV. For pump-probe spectroscopy, the temporal profile of the picosecond X-ray laser was measured by cross correlation technique. The sideband spectra associated with infrared two-photon absorption by the Xe $4d$ $j = 5/2$ photoelectrons have been measured for various time delays of the IR probe pulse relative to the X-ray pump. The pulse width of the X-ray laser was found to be 5.7 ps. That width is in reasonable agreement with the value estimated using an X-ray streak camera.

ACKNOWLEDGEMENTS

This work was supported by a Grant-in-Aid for Scientific Research B (No. 26286078) from the Japanese Society for the Promotion of Science. We thank the JAEA X-ray laser research group for laser operations. This work was performed under the shared use program of JAEA Facilities.

[1] P. Carroll, E. Kennedy, and G. O'Sullivan, IEEE J. Quantum Electronics **QE19**, 1807 (1983).
[2] J. Bridges, C. Cromer, and T. Mcllrath, Appl. Opt. **25**, 2208 (1986).
[3] Z. Zhang *et al.*, Opt. Exp. **19**, 4562 (2011).
[4] C. Rischel *et al.*, Nature **390**, 490 (1997).
[5] C.W. Siders *et al.*, Science **286**, 1340 (1999).
[6] T. Lee *et al.*, Proc. SPIE **4978**, 77 (2003).
[7] R. Frankel, Science **204**, 622 (1979).
[8] C. Laperle *et al.*, Appl. Phys. Lett. **91**, 173901 (2007).
[9] M. Nishikino *et al.*, Rev. Sci. Instrum. **81**, 026107 (2011).
[10] K. Sato *et al.*, Radiat. Res. **174**, 436 (2010).
[11] M. Jurvanssu, A. Kivimäki, and S. Aksela, Phy. Rev. A **64**, 012502 (2001).
[12] L.D. van Woerkom, R. R. Freeman, S. Davey, W. E. Cooke, and T. J. McIlrath, *High-Energy Density Physics with Subpicosecond Laser Pulses*, Vol. 17 of 1989 SAS Technical Digest Series (Optical Society of America, Washington, D.C, 1989), postdeadline paper PDP3.
[13] J. M. Schins *et al.*, Phys. Rev. Lett. **73**, 2180 (1994).
[14] A. Cionga and V. Florescu, Phys. Rev. A **47**, 1830 (1993).
[15] J. Itatani *et al.*, Phys. Rev. Lett. **88**, 173903 (2002).
[16] M. Hentschel *et al.*, Nature **414**, 509 (2001).
[17] P. Kruit and F. Read, J. Phys. E **16**, 313 (1983).
[18] A. Matsuda *et al.*, Rev. Sci. Instrum. **82**, 103105 (2011).
[19] M. Mucke *et al.*, Rev. Sci. Instrum. **83**, 063106 (2012).
[20] T. Kawachi *et al.*, Phys. Rev. A **66**, 033815 (2002).
[21] Y. Ochi *et al.*, Appl. Phys. B **78**, 961 (2004).
[22] M. Nishikino *et al.*, Phys. Rev. A **68**, 061802 (R) (2003).
[23] Y. Ochi *et al.*, Appl. Opt. **46**, 1500-1506 (2007).
[24] P. Lablanquie *et al.*, Phys. Rev. Lett. **87**, 053001 (2001).
[25] D. M. Holland *et al.*, J. Phys. B: At. Mol. Opt. Phys. **12**, 2465 (1979).
[26] A. Kivimäki *et al.*, J. Electron. Spectrosc. Relat. Phenom. **101-103**, 43 (1999).
[27] T. Luhmann *et al.*, Phys. Rev. A **57**, 282 (1998).
[28] C. Bostedt *et al.*, Phys. Rev. Lett. **100**, 133401 (2008).
[29] S. Namba *et al.*, Phys. Rev. A **84**, 053202 (2011).
[30] N. Kroll and K. Watson, Phys. Rev. A **8**, 804 (1973).
[31] A. Maquet and R. Taïeb, J. Mod. Opt. **54**, 1847 (2007).
[32] H. Reiss, Phys. Rev A **22**, 1786 (1980).